Int. J. Multiphase Flow Vol. 14, No. 3, pp. 265–285, 1988
Printed in Great Britain.

0301-9322/88 $3.00 + 0.00

STEAM–WATER ANNULAR FLOW IN A HORIZONTAL DIVIDING T-JUNCTION

J. D. BALLYK,[1] M. SHOUKRI[1] and A. M. C. CHAN[2]

[1]Department of Mechanical Engineering, McMaster University, Hamilton, Ontario L8S 4L7, Canada
[2]Ontario Hydro, Toronto, Ontario, Canada

(*Received* 4 *May* 1987; *in revised form* 5 *January* 1988)

Abstract—The results of an experimental investigation of the separation phenomena in dividing steam–water annular flow in a horizontal T-junction are presented. Measurements included the pressure and void fraction distributions as well as the total flow rate and quality along the inlet and branching legs. A detailed set of experiments were performed enabling the effects of flow split, inlet quality and inlet mass flux on the phase separation and pressure characteristics to be determined. For the annular inlet flow conditions considered herein, total separation was approached when more than 30% of the inlet flow was removed through the branch. At lower branch flow rates, the degree of phase separation was strongly dependent on the branch flow split and inlet quality. The pressure change from the inlet through the run of the T-junction was modelled using an axial momentum balance at the junction for both homogeneous and separated flow assumptions. The separated flow momentum correction factor was found to be distributed around a value of unity indicating that the axial momentum carried by the branching flow was relatively insignificant. The pressure change from the inlet through the branch was modelled using a balance of mechanical energy for the branching flow which consisted of reversible and irreversible components. Accordingly, a two-phase branch loss multiplier was defined and found to be dependent upon the flow split ratio and junction geometry but independent of the inlet conditions.

1. INTRODUCTION

Dividing and combining two-phase flows are encountered in many engineering systems in the power and process industries. A particular case of interest is that of loss-of-coolant accident (LOCA) in nuclear reactor safety analysis. This requires the accurate prediction of phase and pressure distribution for steam–water flow in complex branching conduits. Since the behaviour of two-phase flows in such situations is not well understood, it is commonly assumed that the quality in all downstream legs of a manifold are equal and hence equal to the inlet quality. Experimental evidence indicates that this assumption may be significantly in error. Investigations carried out to date have shown the separation phenomena to be dependent on a variety of hydraulic and geometrical parameters. These include inlet quality, flow regime and mass flux, the system pressure and orientation with respect to gravity and the branch-to-inlet ratios of diameter and flow rate. Most existing experimental data on the subject were obtained for two-phase flow division in simple T-junctions.

In the present work, the results of an experimental investigation into the characteristics of dividing steam–water annular flow are presented. The experimental facility allowed for measured amounts of steam and water to be mixed to thermodynamic equilibrium and delivered to a T-junction test section. All legs of the test section were in the horizontal plane and had equal flow areas. The measurement systems allowed the time-averaged distributions of pressure and void fraction and the flow quality in each leg of the T-junction to be determined. A set of detailed experiments were carried out to isolate the effects of inlet mass flux, inlet quality and branch flow split on the measured parameters for annular inlet flow. The data presented herein covers conditions which were not examined before and, accordingly, contributes to the existing data base on the subject. In referring to existing data and discussing present data, the subscripts 1, 2 and 3 will be used to describe the important flow characteristics in the inlet, run and branch, respectively.

2. LITERATURE SURVEY ON TWO-PHASE FLOW IN HORIZONTAL T-JUNCTIONS

2.1. Phase separation phenomenon

Until recently, most of the data available on two-phase flow in T-junctions were for low-pressure air–water flow. Results from one of the early investigations of the separation phenomena in horizontal T-junctions were presented by Collier (1976). Air–water separation data was presented for an inlet mass flux of 136 kg/m^2 s and inlet qualities in the range 0.02–0.5. These results showed clearly that a large degree of phase separation occurs under most flow conditions with the gas phase preferentially entering the branch. The degree of phase separation was strongly dependent on the inlet quality.

Hong (1978) presented air–water data in the mass flux and quality ranges $15 < G_1 < 80$ kg/m^2 s and $0.25 < x_1 < 0.97$, covering the wavy and annular flow regimes. For most of the inlet conditions and branch extraction rates his results showed the opposite trend with most of the water removed through the branch ($x_3 < x_1$). Johansen (1979) also examined air–water phase separation in a horizontal T-junction in the ranges $69 < G_1 < 841$ kg/m^2 s and $0.5 < x_1 < 1.0$, covering the stratified to annular flow regimes. His results showed both of the previous trends and were dependent upon the inlet mass flux. Inlet flow regime effects were not considered.

Henry (1981) investigated the separation phenomenon with annular air–water flow in a horizontal test section with a branch-to-inlet diameter ratio of 0.2. His data were in the mass flux and quality ranges $200 < G_1 < 850$ kg/m^2 s and $0.1 < x_1 < 0.6$. The data, however, covered a very low range of flow split ratio ($\dot{m}_3/\dot{m}_1 \leqslant 0.06$) where $\dot{m}_1$ and $\dot{m}_3$ are the total inlet and branch mass flow rates, respectively. Later Azzopardi & Whalley (1982) reported air–water phase separation data in horizontal and vertical T-junctions with various branch-to-inlet diameter ratios covering the ranges $50 < G_1 < 200$ kg/m^2 s and $0.1 < x_1 < 0.8$. The results of Henry (1981) and Azzopardi & Whalley (1982) showed similar trends. They indicated that for low flow split ratios the rate of liquid removal through the branch ($\dot{m}_{L3}$) will approach a limiting value as the gas removal rate ($\dot{m}_{G3}$) approaches zero. This implies that for small values of flow split the branch quality must be lower than the inlet quality. The branch quality increased with increasing flow split eventually levelling off at some value above that of the inlet. The trend reverses for high flow splits since the branch and inlet qualities must be equal when all of the flow is diverted through the branch.

Based on his results for removal rates $<6\%$ of the total flow and on his observation of a linear relationship between the branch liquid and gas flow rates, Henry (1981) developed a semi-empirical relation for phase separation. In his model, Henry accounted for his result of a limiting liquid removal rate when the gas removal rate reaches zero. Agreement between the model and the experimental results was best for higher qualities. Azzopardi & Whalley (1982), however, analysed their wider range of annular flow data for vertical inlet sections by defining an apparent angle (θ) over which the film flow is extracted as

$$\theta = 2\pi \frac{\dot{m}_{L3}}{\dot{m}_{Lfl}} = 2\pi \frac{\dot{m}_3(1 - x_3)}{\dot{m}_{Lfl}}, \qquad [1]$$

where $\dot{m}_{Lfl}$ is the inlet liquid film flow rate. This value is less than or equal to the inlet liquid flow rate ($\dot{m}_{Ll}$) depending on the amount of liquid entrainment. As a first approximation, it was assumed that the gas and liquid extracted through the branch come from the segment of the inlet tube defined by θ. The portion of gas extracted is then related to θ by

$$\frac{\dot{m}_{G3}}{\dot{m}_{Gl}} = \frac{\dot{m}_3}{\dot{m}_1}\frac{x_3}{x_1} = \frac{\theta - \sin\theta}{2\pi}. \qquad [2]$$

The subscripts L and G in the above equations refer to the liquid and gas, respectively.

Azzopardi & Freeman-Bell (1983) extended this work to include a wider range of diameter ratios. They noted that the effect of branch diameter was best represented by

$$\frac{\theta}{\theta'} = 1.2\left(\frac{d_3}{d_1}\right)^{0.4} \qquad [3]$$

when the portion of gas removed is given by

$$\frac{\dot{m}_{G3}}{\dot{m}_{G1}} = \frac{\theta' - \sin\theta'}{2\pi}. \quad [4]$$

The authors reported that most of the data was predicted to within ±30%, with results from higher inlet qualities deviating most significantly. Extending this model to horizontal inlet flows requires knowledge of the angular distribution of film thickness in the inlet section.

Saba & Lahey (1984) presented air–water data for a horizontal T-junction of equal diameters for three values of mass flux, $G_1 = 1355$, 2041 and 2711 kg/m^2 s and for qualities <0.01. In modelling the phase separation phenomenon, the authors identified eight parameters of interest. These are the inlet, run and branch mass fluxes (G_1, G_2 and G_3, respectively), the inlet, run and branch qualities (x_1, x_2 and x_3, respectively), the pressure change from the inlet through the branch, $(\Delta P_{1-3})_j$, and the pressure change from the inlet through the run, $(\Delta P_{1-2})_j$. Assuming three of these parameters to be specified, five conservation equations are required to obtain a solution. The equations used were based on the simplified mixture model, i.e. mixture continuity, vapour continuity and mixture momentum equations for the run and branch as well as a vapour momentum equation for the branch. Empirical relationships proposed by others were used to close the proposed simplified set of conservation equations. Saba & Lahey's (1984) work was the only one to acknowledge the obvious interdependence of the pressure changes and the corresponding phase separation.

Recently, steam–water data were published by a few investigators. Seeger *et al.* (1986) presented experimental data on air–water and steam–water separation in horizontal junctions of equal diameters. The steam–water data were obtained for high pressures (up to 10 MPa). The data covered the range $500 < G_1 < 7000$ kg/m^2 s and various inlet flow patterns. A simple empirical phase separation correlation was proposed to fit their data in the form

$$\frac{x_3}{x_1} = 5\eta - 6\eta^2 + 2\eta^3 + a\eta(1-\eta)^4, \quad [5]$$

where η represents the flow split ratio (G_3/G_1) and $a = 14.6$ for bubbly flow. For other flow regimes a is given by

$$a = 13.9\left[\left(\frac{\rho_G S_1^2}{\rho_L}\right)^{-0.26} - 1\right], \quad [6]$$

where S_1 is the inlet slip ratio. The parameter a relates the peak of the phase separation curve, $(x_3/x_1)_{max}$, to the ratio of the gas to liquid momentum flux in the inlet section. It should be noted that [5] has the correct limit of $x_3 = x_1$ when $G_3 = G_1$ but not when the system pressure approaches the critical conditions.

More recently, Rubel (1986) presented low-pressure steam–water data for a horizontal T-junction in the ranges $15 < G_1 < 50$ kg/m^2 s, $0.20 < x_1 < 0.80$ and $0.2 < G_3/G_1 < 0.8$, covering the stratified and wavy flow regimes. He observed the branch quality (x_3) to be lower than the inlet quality (x_1) for stratified flow, while x_3 was higher than x_1 for wavy and semi-annular flow within the range tested.

These investigations have shown the degree of phase separation to be strongly dependent on the inlet quality and flow regime. In general, the inlet mass flux has shown little effect.

The work presented herein is the result of an investigation which was started in 1984. It is concerned with steam–water annular flow in a horizontal T-junction with equal diameter legs covering a new range of operating conditions: $400 < G_1 < 1200$ kg/m^2 s, $0 < x_1 < 0.15$ and $0 < \dot{m}_3/\dot{m}_1 < 1.0$. Accordingly, it contributes to the much-needed data base on the subject. Another, unique feature of the present work is that it includes data on the void fraction distribution which will aid in the development of detailed mechanistic models in the future.

2.2. Pressure distribution characteristics

It is well-established that when a single-phase or two-phase flow is divided in a T-junction, the flow in the axial direction through the run of the T experiences a pressure rise due to flow expansion. A pressure drop is generally experienced by the flow turning through the branch because

of significant irreversible losses which are typically higher than the associated Bernoulli-type pressure rise. Most methods suggested in the literature for predicting these pressure changes are direct extensions of methods used for single-phase flow. These are based on a simple momentum or energy balance on the junction as a control volume, as shown by Collier (1976).

For a T-junction in which the inlet and run have equal areas and the average fluid properties are assumed to define the flow field, a single-phase axial momentum balance may be written as

$$(\Delta P_{2-1})_j = P_{2j} - P_{1j} = k_{1-2}(u_1^2 - u_2^2)\rho, \quad [7]$$

where P_{1j} and P_{2j} are the junction inlet and run pressures and u_1 and u_2 are the average inlet and run velocities. The coefficient k_{1-2} accounts for the indeterminant axial momentum carried out of the control volume by the branching flow. Alternatively, a loss coefficient, $\bar{k}_{1-2}$, can be defined based on a Bernoulli-type model to account for reversible and irreversible pressure changes, i.e.

$$(\Delta P_{2-1})_j = P_{2j} - P_{1j} = \frac{\rho}{2}(u_1^2 - u_2^2) - \bar{k}_{1-2}\frac{\rho}{2}u_1^2. \quad [8]$$

The first term on the r.h.s. of [8] is the reversible run pressure rise and the second term is the irreversible pressure loss modelled in terms of the inlet dynamic head.

By considering the two-phase flow to be a homogeneous mixture in which the two phases have equal velocities, the mixture density (ρ_H) and velocity (u_H) may be written as

$$\rho_H = \frac{\rho_G \rho_L}{x\rho_L + (1-x)\rho_G} \quad [9]$$

and

$$u_H = \frac{G}{\rho_H}, \quad [10]$$

respectively; where G is the total flux. Substituting [9] and [10] into [7] yields a homogeneous model for the run pressure rise, i.e.

$$(\Delta P_{2-1})_j = k_{(1-2)H}[(\rho_H u_H^2)_1 - (\rho_H u_H^2)_2], \quad [11]$$

where $k_{(1-2)H}$ is the homogeneous momentum correction factor.

By considering the flow of each phase separately and introducing $k_{(1-2)s}$, the separated flow momentum correction factor, [11] becomes

$$(\Delta P_{2-1})_j = k_{(1-2)s}\left\{\left[\frac{G_1^2 x_1^2}{\rho_G \alpha_1} + \frac{G_1^2(1-x_1)^2}{\rho_L(1-\alpha_1)}\right] - \left[\frac{G_2^2 x_2^2}{\rho_G \alpha_2} + \frac{G_2^2(1-x_2)^2}{\rho_L(1-\alpha_2)}\right]\right\}, \quad [12]$$

where α_1 and α_2 are the void fractions in the inlet and run sections of the T-junction, respectively.

Fouda (1975) and Fouda & Rhodes (1974) investigated air–water annular flow in a 50.8 mm dia inlet tube with a 25.4 mm vertical branch. The data obtained was analysed based on [11] and [12]. The authors suggested that the separated flow model be used for simple T-junctions with a momentum correction factor $k_{(1-2)s} = 0.533$.

Fouda & Rhodes (1974) modelled the radial pressure drop through the branch by treating the braching port as an orifice. Assuming a homogeneous mixture, the orifice equation yielded

$$\dot{m}_3 = C_{th} A_3 [2\rho_{H3}(\Delta P_{1-3})_j]^{1/2}, \quad [13]$$

where $\dot{m}_3$ is the total branch mass flow rate, C_{th} is the two-phase homogeneous discharge coefficient and the subscript 3 refers to the branch conditions. The data presented suggested that the orifice model best represented the experimental results with a homogeneous discharge coefficient $C_{th} = 1.22$.

Other methods for predicting the pressure changes through the branch were developed from the usual method used for single-phase flow, which is based on dividing the branch pressure change, $(\Delta P_{1-3})_j$, into reversible and irreversible components. As shown by Collier (1976), for single-phase flow, this method yields

$$(\Delta P_{1-3})_j = P_{1j} - P_{3j} = \frac{\rho}{2}(u_3^2 - u_1^2) + k_{1-3}\frac{\rho u_1^2}{2}, \quad [14]$$

where the first term on the r.h.s. represents the reversible component and the second term is the irreversible component modelled in terms of the inlet dynamic head. This model was extended by Saba & Lahey (1984) who showed that for separated two-phase flow [14] can be written as

$$(\Delta P_{1-3})_j = \frac{\rho_{H3}}{2}\left[\frac{G_3^2}{(\rho_3''')^2} - \frac{G_1^2}{(\rho_1''')^2}\right] + \frac{k_{1-3}}{2}\frac{G_1^2}{\rho_L}\Phi, \quad [15]$$

where k_{1-3} is the single-phase loss coefficient based on the same flow split (G_3/G_1), Φ is a two-phase flow multiplier and the energy density (ρ''') is defined by

$$\frac{1}{(\rho''')^2} = \left[\frac{(1-x)^3}{\rho_L^2(1-\alpha)^2} + \frac{x^3}{\rho_G^2\alpha^2}\right]. \quad [16]$$

A homogeneous model was obtained by replacing the energy densities in [15] with the appropriate homogeneous density given by [9]. The authors reported good agreement between experimentally measured values and the homogeneous model.

The work of Saba & Lahey (1984) and Reimann & Seeger (1986) differ essentially in their respective recommendations for the value of Φ to be used with [15]. Saba & Lahey (1984) suggested that a two-phase multiplier be used in the form

$$\Phi_s = \frac{\rho_L}{\rho'}, \quad [17]$$

where ρ' is the momentum density given by

$$\frac{1}{\rho'} = \left[\frac{x^2}{\alpha\rho_G} + \frac{(1-x)^2}{(1-\alpha)\rho_L}\right]. \quad [18]$$

For the homogeneous assumption, the momentum density reduces to the homogeneous density (ρ_H) and [17] becomes

$$\Phi_H = \frac{\rho_L}{\rho_H}. \quad [19]$$

This formulation yields a homogeneous multiplier that is independent of flow split, a strong function of inlet quality and generally higher than that determined in the present work.

Reimann & Seeger (1986) used the homogeneous model as well, however, their multiplier can be reduced to

$$\Phi_H = \frac{\rho_L\rho_{H3}}{\rho_{H1}^2}, \quad [20]$$

which is a function of flow split and inlet quality.

3. EXPERIMENTAL ARRANGEMENTS

3.1. Experimental facility

The steam–water loop used in the present work is shown schematically in figure 1. The system consists of a 2 hp progressive cavity pump supplied from a 450 l. hot water storage tank. The inlet water flow is controlled by way of valves located in the main water line and loop bypass. From the pump, the water flows to a 6 kW circulation heater and is then passed through a filter capable of removing particles to 10 μm dia. From the filter, the water flows through a check valve to the two-phase mixer. Steam is taken from the main supply at approx. 1 MPa and is reduced to the desired pressure though a pressure regulator. The steam flow rate is measured by an orifice meter and the steam is delivered to the two-phase mixer where it is combined with the inlet water.

Upon leaving the mixer, the two-phase flow becomes fully developed and reaches thermodynamic equilibrium through a 3.6 m long section of 25.4 mm sch. 40 stainless steel pipe before reaching the test section. The test section used in these experiments was a T-junction with all legs in the horizontal plane. The T was made up of a 25.65 mm i.d. inlet with a 25.65 mm i.d. branch. At the junction the flow is split into two streams; one in the axial direction through the run of the T, the other in the radial direction through the branch. At the outlet from each leg, the steam–water

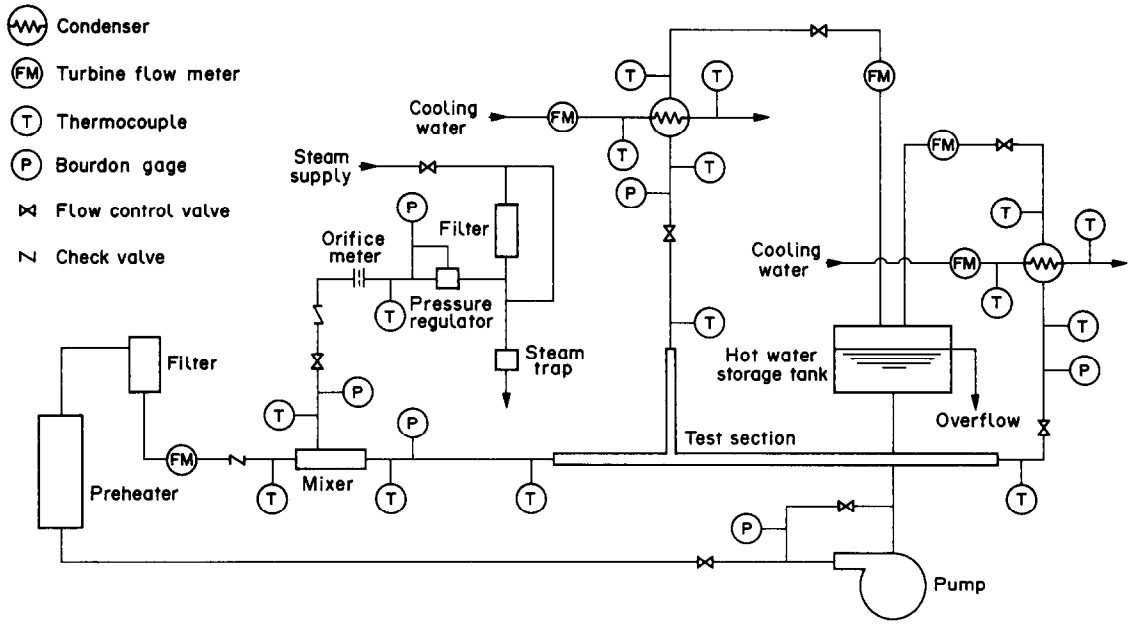

Figure 1. Schematic diagram of the steam–water loop.

mixture enters a 50 kW, multipass, shell and tube condenser exiting as single-phase water. There are two flow control valves located in each branch of the T, one upstream and one downstream of the condensers. The condensate from each branch is then directed back to the storage tank. The water level in the tank is kept constant by means of an open overflow. The entire loop and tank are insulated.

The test section used for these experiments consisted of a horizontal tube with one horizontal branch carefully machined and welded at 90° to ensure a sharp-edged opening. The test section was constructed of 31.75 mm o.d., 25.65 mm i.d. stainless steel tubing. The entrance to the test section was fitted with a 0.15 m long section of transparent tubing for identification of the inlet flow regime. The inlet section and the branch were of equal length (610 mm) while the run was 2300 mm long to ensure fully developed flow within the test section downstream of the junction.

3.2. Measurements

Water flow rates were measured with turbine flow meters at five locations throughout the loop as shown in figure 1. The steam flow rate was measured using a calibrated orifice plate assembly equipped with condensing chambers. Temperature measurements were made using type E thermocouples at 15 locations throughout the loop, as shown in figure 1. Detailed pressure and void fraction distributions along the three legs of the test section were obtained.

Figure 2a shows the test section with the pressure tap locations. Five pressure taps were located in each of the inlet and branch sections. Due to a slower flow development, the run contained 15 pressure taps to ensure a fully developed profile was obtained. At each tap location, a 1.6 mm hole was drilled through the tube wall and countersunk to accept a 6.4 mm stainless steel tube. Short pieces of tubing were then bent and silver soldered into place for connecting the taps to the pressure measurement system, as shown in figure 2b. Special care was taken in drilling and polishing the taps to ensure no burrs protruded into the flow area. All taps were located at the bottom of the test section to inhibit steam from entering the pressure lines.

The first upstream pressure tap in the inlet section was used as a reference. Its signal was split with one branch connected to the high side of a differential pressure transducer for measuring system pressure. The low side of this transducer was open to the atmosphere. The other branch was connected to the high side of a bank of two differential pressure transducers, one high range and one low range, used for measuring the pressure differences between the reference station and subsequent stations. The signals from all other pressure taps were delivered individually to the low

side of the transducer bank through a 24-channel switching valve. These signals can be directed to the high range (0–50 kPa) or low range (0–0.5 kPa, single-phase; 0–5.0 kPa, two-phase) transducers through a series of valves. Pressure lines from the taps to the transducer bank were made of Tygon tubing. A simple purging system was used to ensure that the lines were always free of vapour or air. The output from the differential pressure transducers was time averaged to obtain the required pressure differences.

Void fraction measurements were made at various locations throughout the test section with a traversing single-beam gamma densitometer. The system consisted of a 75 mCi ^{57}Co sealed source and the signal was received by a 76.2 mm cubic NaI(Tl) scintillator and standard signal processing equipment arranged to operate in the count mode. The source, collimating plates and scintillator were housed in a carriage capable of scanning the test section on a traversing table. Void fraction measurements were made at 17 stations throughout the test section, as shown in figure 2a.

All signals from the flow meters, thermocouples, pressure transducers and the gamma densitometer were directed to a computer-based Taurus One data acquisition system. The system was hosted by an IBM-PC equipped with two floppy disk drives and a 10 Mbyte hard disk used for data storage and analysis.

Details of the experimental facility and measuring equipment and its calibration and accuracy were reported by Ballyk (1986).

3.3. Data reduction and test conditions

The inlet, branch and run qualities were determined from energy balances within the loop. Accordingly, the reported flow qualities are the thermodynamic equilibrium qualities. With the measurement systems described, it was possible to check both the mass and energy balances across the test section for most flow conditions. For these runs, the results showed that 90% of the measurements satisfied the balances within the following ranges: $\pm 1.0\%$ for total mass; $\pm 1.5\%$ for total energy; $\pm 6.0\%$ for steam; and $\pm 1.0\%$ for water.

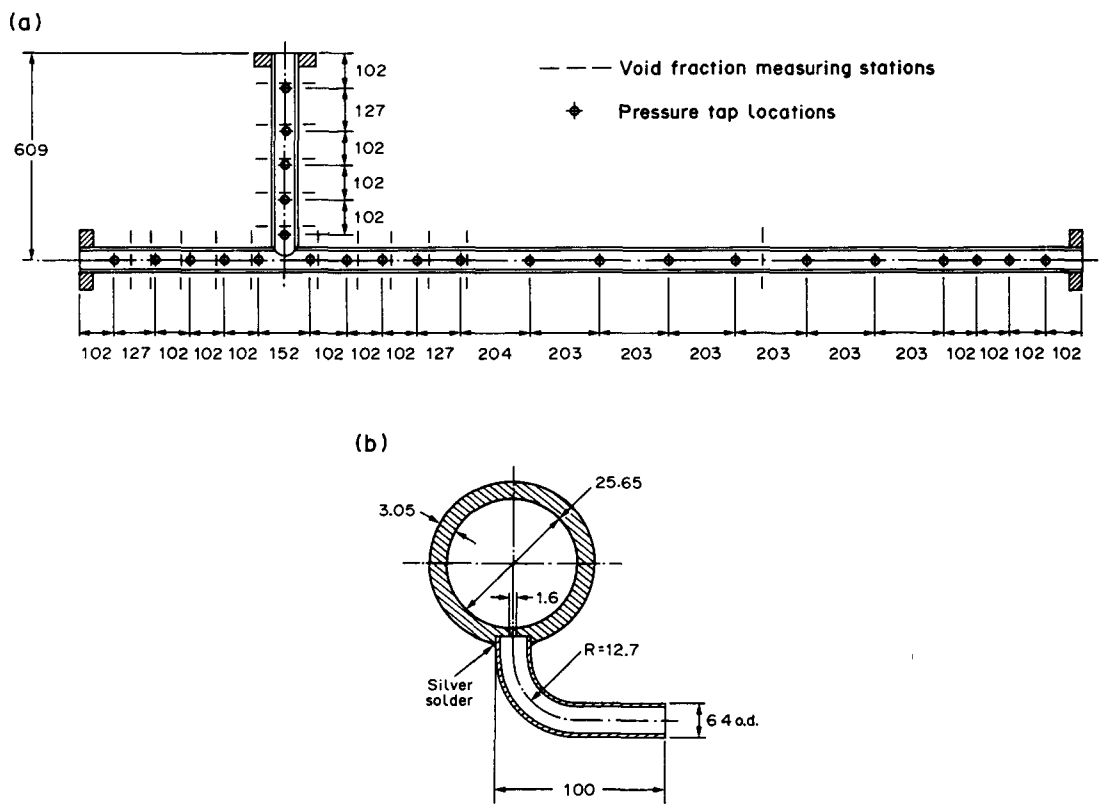

Figure 2. Schematic diagram of the test section (all dimensions in mm). (a) Pressure and void fraction measuring stations; (b) tap assembly.

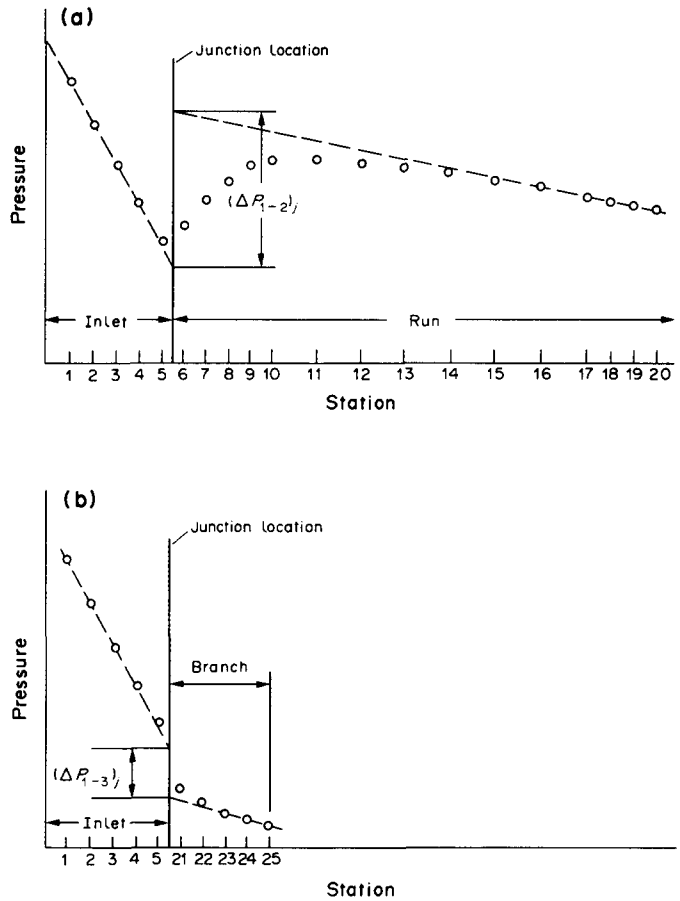

Figure 3. Schematic diagram of a typical pressure distribution in dividing flow: (a) run pressure differential $(\Delta P_{1-2})_j$; (b) branch pressure differential $(\Delta P_{1-3})_j$.

The junction pressure rise in the run, $(\Delta P_{1-2})_j$, and pressure drop in the branch, $(\Delta P_{1-3})_j$, were obtained by extrapolating the fully developed pressure profiles in each leg to the junction by the least-squares method. The procedure is shown schematically in figure 3. Pressure differences were measured for both single-phase water and two-phase, steam–water flow.

The steam–water data presented herein were obtained from 64 runs covering the test conditions summarized in table 1. The loop design provided enough flexibility to control the flow split ratio (G_3/G_1) for a given inlet quality and mass flux. For the test conditions given in table 1 the flow split was varied to cover the range 0.075–1.0. All of these data corresponded to the annular flow regime as confirmed by visual observation through the small transparent section preceding the test section. In all cases the inlet pressure was <250 kPa. The experimental results obtained in the present work are shown in table 2.

Table 1. Two-phase test conditions

Inlet quality, x_1 (%)	Inlet mass flux, G_1 (kg/m^2 s)			
	450	600	900	1200
2.0		X	X	X
4.5	X	X	X	
8.0		X		
15.2	X			

Table 2. Experimental results

$\frac{\dot{m}_3}{\dot{m}_1}$	G_1 (kg/m^2 s)	x_1	$\frac{x_3}{x_1}$	α_1	α_2	α_3	$(\Delta P_{2-1})_j$ (kPa)	$(\Delta P_{1-3})_j$ (kPa)	P_1 (kPa)
0.115	445.9	0.051	1.56	0.884	0.892	0.867	0.685	−0.068	128
0.149	439.9	0.049	2.57	0.866	0.894	0.886	1.009	0.042	119
0.189	431.9	0.051	3.71	0.879	0.874	0.918	1.532	0.660	111
0.230	450.5	0.046	3.60	0.854	0.865	0.923	1.488	0.589	141
0.386	451.7	0.044	2.60	0.851	0.059	0.917	3.273	1.307	117
0.664	459.0	0.043	1.47	0.908	0.120	0.846	3.075	2.168	123
1.000	450.7	0.046	0.95	0.907	—	0.898	2.340	3.598	137
0.077	446.8	0.151	2.58	0.977	0.977	0.957	2.693	0.004	185
0.105	454.4	0.152	2.88	0.991	0.992	0.968	4.877	0.379	169
0.160	447.5	0.153	3.34	0.976	0.949	0.982	8.241	2.489	130
0.220	454.6	0.153	3.09	0.981	0.976	0.976	9.755	4.921	132
0.297	452.4	0.152	2.72	0.988	0.976	0.969	11.580	7.302	148
0.453	450.6	0.152	2.16	0.987	0.948	0.984	11.023	11.923	171
0.603	442.7	0.152	1.62	0.979	0.039	0.979	11.303	14.999	184
1.000	411.1	0.148	0.97	0.983	—	0.955	9.580	17.694	203
0.073	601.5	0.019	0.78	0.804	0.801	0.909	0.240	−0.120	130
0.160	583.8	0.023	2.73	0.806	0.816	0.895	0.546	0.271	117
0.168	588.4	0.021	4.32	0.790	0.685	0.901	0.609	0.494	112
0.222	593.6	0.024	4.35	0.808	0.739	0.909	0.810	1.027	117
0.402	620.6	0.018	2.47	0.804	0.187	0.860	1.839	1.015	114
0.708	583.4	0.025	1.41	0.803	0.080	0.813	2.096	1.984	125
1.000	602.2	0.022	1.03	0.816	—	0.848	2.071	2.837	139
0.095	598.7	0.042	0.90	0.861	0.873	0.921	0.963	−0.184	152
0.125	596.1	0.044	2.74	0.878	0.885	0.933	1.419	−0.016	137
0.141	591.8	0.046	2.73	0.886	0.852	0.906	1.532	0.201	132
0.178	598.9	0.045	3.66	0.879	0.867	0.923	2.143	0.839	118
0.218	598.1	0.044	4.00	0.874	0.766	0.989	3.641	1.332	119
0.264	597.5	0.045	3.88	0.890	0.067	0.966	7.708	2.178	126
0.311	609.0	0.050	3.21	0.926	0.072	0.874	8.459	2.544	142
0.370	594.6	0.047	2.65	0.905	0.045	0.932	8.156	2.845	126
0.453	593.5	0.048	2.20	0.889	0.020	0.927	8.090	3.626	131
0.673	596.0	0.045	1.50	0.865	0.031	0.903	6.478	4.172	141
1.000	610.1	0.044	0.99	0.883	—	0.922	4.560	6.360	164
0.081	600.6	0.079	1.24	0.889	0.903	0.850	1.613	−0.351	194
0.122	593.5	0.080	2.45	0.876	0.935	0.931	2.689	0.057	163
0.154	597.1	0.079	2.78	0.908	0.942	0.940	4.099	0.782	145
0.200	596.6	0.082	2.92	0.944	0.898	0.948	5.541	2.381	123
0.269	598.1	0.084	3.06	0.975	0.875	0.946	8.339	4.300	138
0.325	594.1	0.081	2.86	0.925	0.878	0.967	8.343	5.920	145
0.456	601.3	0.078	2.17	0.940	0.104	0.946	9.265	8.469	155
0.808	596.6	0.080	1.21	0.864	0.037	0.919	9.873	11.903	189
1.000	599.9	0.078	0.97	0.935	—	0.942	9.250	13.459	206
0.107	901.6	0.021	1.39	0.749	0.781	0.860	0.806	0.362	158
0.140	892.4	0.020	3.38	0.780	0.781	0.939	1.216	0.266	143
0.180	907.5	0.019	4.17	0.787	0.787	0.921	1.346	0.731	128
0.242	901.9	0.019	4.00	0.779	0.060	0.914	4.144	1.465	137
0.314	907.6	0.019	3.01	0.776	0.131	0.926	4.579	1.940	130
0.490	896.6	0.020	2.07	0.784	0.086	0.882	4.815	3.354	134
0.664	906.9	0.019	1.53	0.784	0.076	0.835	3.952	3.969	147
1.000	898.1	0.019	0.97	0.807	—	0.845	3.538	4.852	180
0.125	873.0	0.044	2.04	0.831	0.922	0.892	2.048	0.030	192
0.147	901.2	0.044	2.27	0.911	0.901	0.874	2.720	0.380	182
0.222	888.8	0.043	3.07	0.888	0.900	0.942	4.792	2.478	128
0.294	890.7	0.043	3.40	0.824	0.220	0.956	11.930	5.027	143
0.357	905.9	0.043	2.76	0.913	0.122	0.936	13.815	5.892	150
0.445	902.9	0.043	2.21	0.864	0.154	0.921	13.265	6.913	161
0.608	883.8	0.043	1.62	0.905	0.185	0.900	11.401	8.145	176
1.000	826.6	0.043	1.00	0.869	—	0.898	7.210	10.928	212
0.122	1189.4	0.019	1.90	0.780	0.852	0.880	1.249	0.488	199
0.169	1194.2	0.020	3.03	0.809	0.847	0.906	1.722	0.829	165
0.218	1191.2	0.020	3.64	0.772	0.799	0.935	2.159	2.021	136
0.267	1189.5	0.020	3.57	0.769	0.062	0.921	8.534	3.981	133
0.398	1198.5	0.020	2.42	0.778	0.111	0.901	7.695	5.511	147
0.655	1196.7	0.020	1.55	0.779	0.053	0.894	6.453	6.402	181

4. PHASE SEPARATION AND REDISTRIBUTION

4.1. Results and discussion

The phase separation data are presented in figures 4–8. The branch quality, normalized with respect to the inlet quality (x_3/x_1), is plotted against the branch flow split ($\dot{m}_3/\dot{m}_1$) for fixed nominal values of inlet mass flux (G_1) and quality (x_1). Equal phase distribution is represented by the horizontal line $x_3/x_1 = 1.0$. Complete phase separation, which corresponds to all of the inlet vapour removed through the branch, is represented by the inverse of the branch flow split, i.e. $x_3/x_1 = \dot{m}_1/\dot{m}_3$. Figures 4–8 clearly show the severe phase maldistribution which can occur in the downstream legs of the T. The assumption of equal phase distribution does not approximate the measured data for annular flow in any region. At low branch flow splits, the branch quality increases very rapidly with increasing flow split crossing the equal phase distribution line at close to 90°. If the data in this region was extrapolated back to the horizontal axis it appears that some limiting value of water flow could be established in the branch when the branch quality is reduced to zero. This supports the findings of Azzopardi & Whalley (1982) and Henry (1981) and suggests that the liquid is first removed from the low velocity film flowing at the tube wall in line with the branching port.

When the flow split is further increased, the branch quality peaks or levels off at flow splits in the range of 20–30%. As expected, the branch quality eventually decreases to the inlet quality when $\dot{m}_3/\dot{m}_1 = 1$. In all cases, when the flow split ratio exceeds 30–40%, the branch quality is closely approximated by the complete separation curve. This trend was observed by Saba & Lahey (1984) for air–water flow in a horizontal T section. For experiments in which no less than 30% of the total flow was removed through the branch, they reported branch qualities in the range of total phase separation that decreased with increasing flow split. Since these experiments were carried out using air–water flow with lower inlet qualities than the present work ($\leqslant 1.0\%$) and in all cases the inlet flow regimes were slug or stratified, no direct comparison of the results can be made.

Figure 4–6 show the branch phase separation ratio plotted against flow split for a constant inlet mass flux and varying inlet quality. In all cases, an increase in inlet quality reduces the peak phase separation ratio and increases the flow split at which complete separation takes place. It has been suggested by Azzopardi & Whalley (1982) and Seeger *et al.* (1986) that these observations may be explained in terms of the effect of quality variations on the distribution of the phases within the

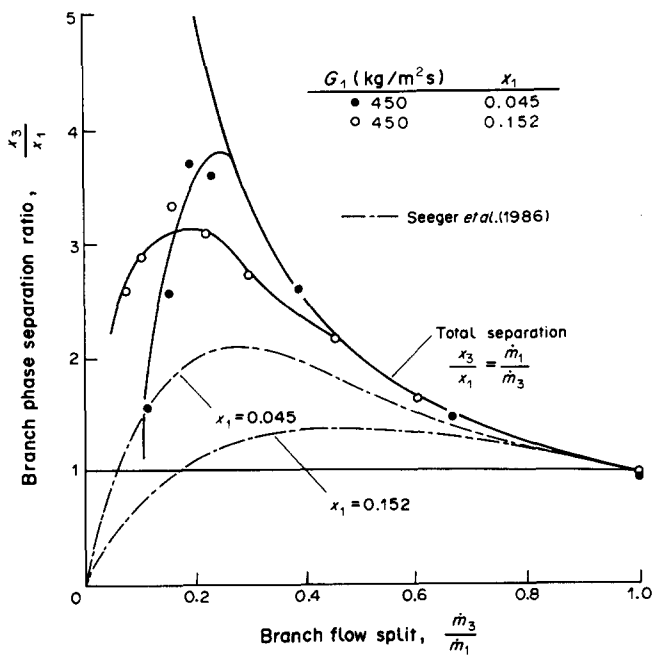

Figure 4. Branch phase separation ratio vs flow split, effect of inlet quality ($G_1 = 450$ kg/m² s).

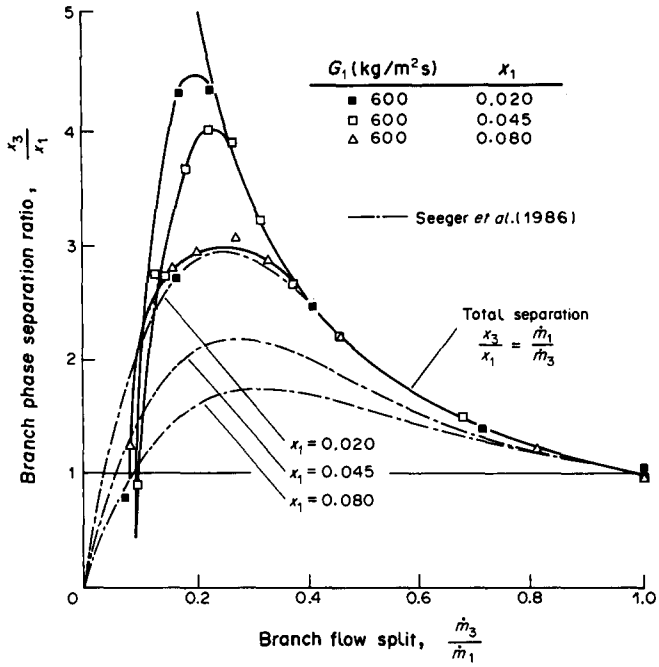

Figure 5. Branch phase separation ratio vs flow split, effect of inlet quality ($G_1 = 600$ kg/m² s).

tube cross-section and the relative distribution of axial momentum between the two phases. Increasing quality at constant mass flux in the annular flow, which corresponds to increasing vapour superficial velocity, causes more of the liquid film to be swept up the sides of the tube from the thick layer of liquid on the bottom. As a result, more of the liquid film is readily available for extraction. This may be verified with data collected from test sections having smaller branch-to-inlet diameter ratios and with measurements of the angular distribution of film thickness in the inlet cross-section.

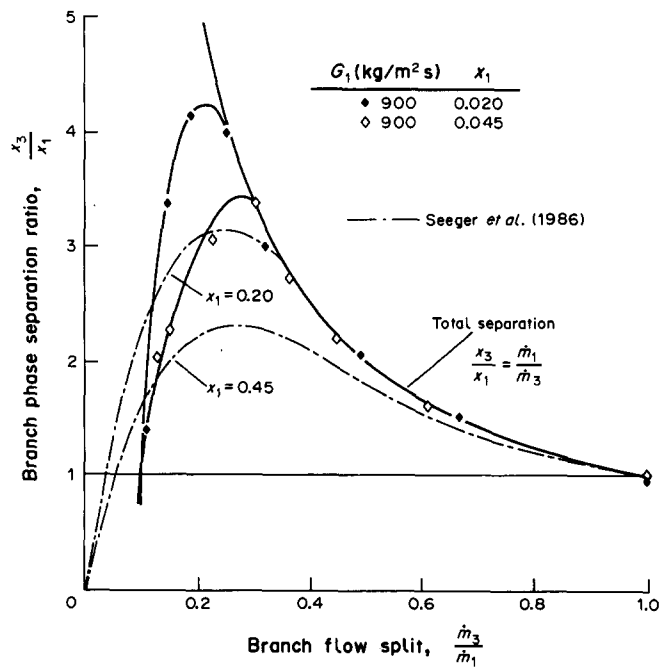

Figure 6. Branch phase separation ratio vs flow split, effect of inlet quality ($G_1 = 900$ kg/m² s).

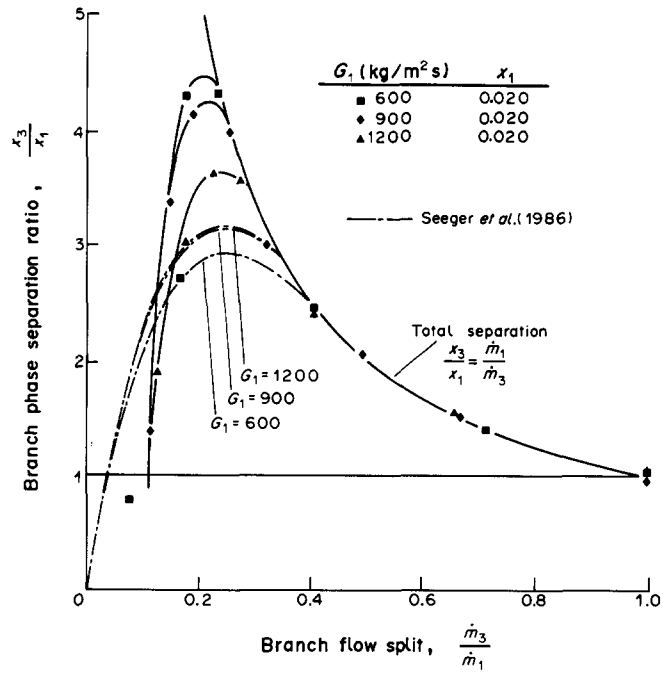

Figure 7. Branch phase separation ratio vs flow split, effect of inlet mass flux ($x_1 = 0.020$).

Figures 7 and 8 show the branch phase separation ratio plotted against branch flow split for fixed inlet quality at varying inlet mass flux. For the range of data tested the effect of inlet mass flux variation is less significant than that of inlet quality. The point of total separation is somewhat independent of mass flux. The peak separation ratio appears to be slightly lower for the higher values of inlet mass flux (900 and 1200 kg/m²).

It is interesting to examine the void fraction and pressure profiles in the T section as it may provide some insight into the phase separation phenomenon. Figures 9a and 9b show the void

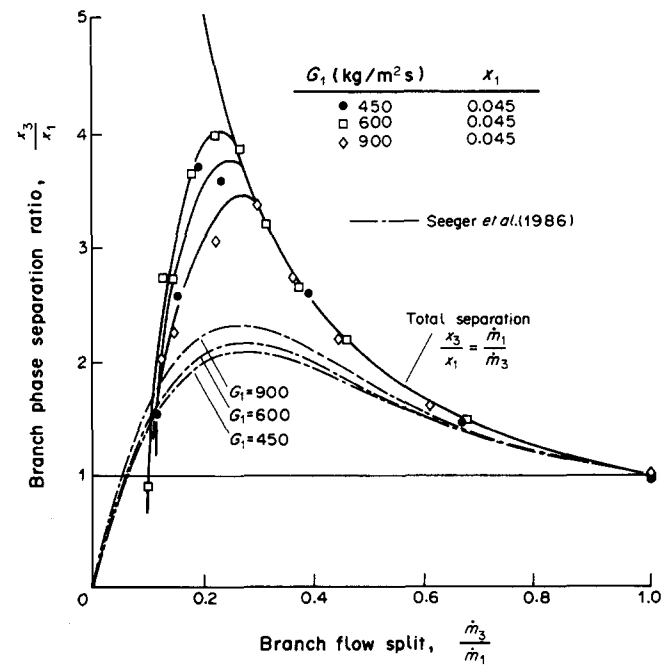

Figure 8. Branch phase separation ratio vs flow split, effect of inlet mass flux ($x_1 = 0.045$).

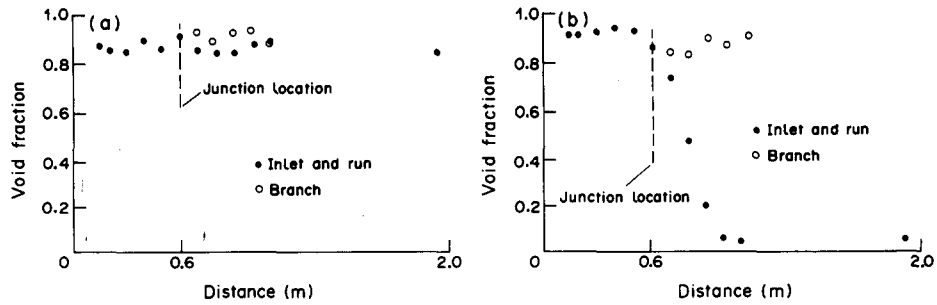

Figure 9. Typical void fraction distributions near total separation: (a) $G_1 = 600\ \text{kg/m}^2\,\text{s}$, $x_1 = 0.045$, $\dot{m}_3/\dot{m}_1 = 0.18$; (b) $G_1 = 600\ \text{kg/m}^2\,\text{s}$, $x_1 = 0.050$, $\dot{m}_3/\dot{m}_1 = 0.31$.

fraction profiles for similar inlet conditions but with different flow split ratios. These correspond to a value below that required for total phase separation ($\dot{m}_3/\dot{m}_1 = 0.18$) in figure 9a and a condition where almost total phase separation took place ($\dot{m}_3/\dot{m}_1 = 0.31$) in figure 9b. The corresponding pressure data is shown in figures 10a and 10b. It can be seen in figure 9b, where almost all the vapour was vented through the branch, that the void fraction in the inlet leg increases as the junction is approached. This corresponds to deceleration of the vapour phase as it tries to turn through the branch. The drastic change in the fully developed run void fraction between figures 9a and 9b was associated with a flow regime transition from annular towards the slug/plug flow regime as total separation was approached. Under these conditions, the void fraction through the run remained relatively high for some distance downstream of the junction. Figure 10b shows a very steep positive pressure gradient in this portion of the run. These measurements suggest the presence of significant phase redistribution and vapour recirculation in the run downstream of the junction as the vapour responds to this adverse pressure gradient. This explains the need for a long recovery length in the run, as reported by Saba & Lahey (1984) and observed in the present work. It should be noted that the measured branch and run qualities corresponding to figure 9a were 0.166 and 0.023, respectively, and those corresponding to figure 9b were 0.161 and 0.002, respectively.

The present data trends seem to support those observed in previous studies. At low branch flow splits most of the branching flow is removed from the liquid film flowing in line with the branching port. As a result, this portion of the separation curve is characterized by a branch quality below that of the inlet. Increasing the flow split, which corresponds to lowering the downstream pressure in the branch, is simultaneously associated with an increase in pressure rise through the run of the T-junction due to flow expansion. This adverse pressure gradient yields an additional force driving the flow through the branch. The gas phase can respond more readily to the favourable pressure gradient in the branch and the adverse gradient in the run due to its lower axial momentum. As a result, this portion of the curve is characterized by a steep increase in the branch quality until total separation is reached. The region of complete phase separation is associated with significant phase redistribution in the run causing a flow regime transition. In order to examine and quantify

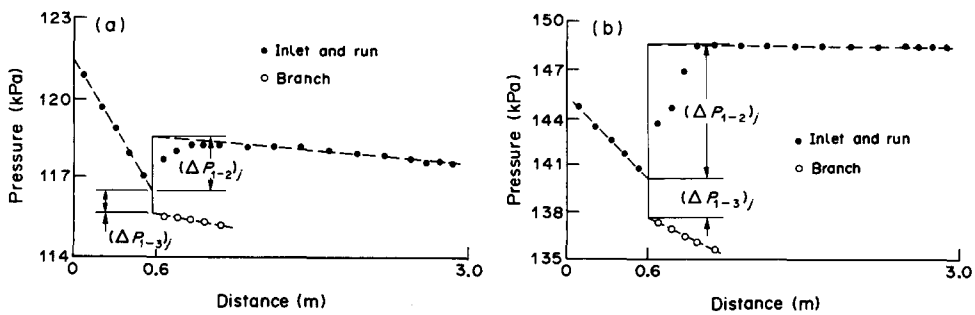

Figure 10. Typical pressure distributions near total separation: (a) $G_1 = 600\ \text{kg/m}^2\,\text{s}$, $x_1 = 0.045$, $\dot{m}_3/\dot{m}_1 = 0.18$; (b) $G_1 = 600\ \text{kg/m}^2\,\text{s}$, $x_1 = 0.050$, $\dot{m}_3/\dot{m}_1 = 0.31$.

the different parameters associated with the above simplified physical model, data on the distribution of the phases in the inlet leg are needed. Work is currently underway to obtain simultaneous data on the liquid film distribution in the inlet cross-section.

The void fraction profiles obtained from all the experiments performed in the present work exhibited features similar to those shown in figures 9a and 9b.

4.2. Comparison with existing models and correlations

The phase separation data obtained in the present work were compared with the model developed by Azzopardi and co-workers (Azzopardi & Whalley 1982; Azzopardi & Freeman-Bell 1983) ([1]–[4]) and with the empirical relationship recently presented by Seeger *et al.* (1986), i.e. [5] and [6].

Azzopardi & Whalley's model, developed for annular flow, requires knowledge of the liquid film flow rate or the liquid entrainment rate in the inlet section. For a horizontal inlet, this model also requires knowledge of the angular distribution of film thickness in the inlet section. Since only the total inlet liquid flow rate was measured in the present experiments, the experimental data were compared with the model predictions using the entrainment ratio, $E = (1 - m_{Lf1}/m_{L1})$, as a parameter and an assumption of uniform film thickness. The results showed that the model can qualitatively predict the shape of the phase separation curves. Quantitatively, the model underpredicts the level of phase maldistribution observed in the present work and underestimates the effect of inlet quality. Assuming unrealistically high entrainment rates can, however, bring the model predictions closer to the measured values. Since this model was originally developed for vertical annular flow where the momentum of the liquid film and gas core are similar in magnitude, disagreement with the present work is not unexpected.

Shown also in figures 4–8 is the empirical correlation developed by Seeger *et al.* (1986). This correlation generally underpredicts the current data but is capable of capturing the observed parametric trends. This model was developed for higher-pressure flows which may account for the discrepancy.

The above comparisons suggest that further work is needed to develop a more generalized model capable of quantitatively predicting the phase separation phenomenon in piping junctions under two-phase annular flow conditions.

5. PRESSURE CHANGES AT THE JUNCTION

5.1. Single-phase flow

Pressure distribution data for single-phase water flow were obtained for different mass fluxes and for split ratios ($\dot{m}_3/\dot{m}_1$) covering the range 0.1–1.0. The pressure distribution in each leg was extrapolated to obtain the junction pressure differences $(\Delta P_{1-2})_j$ and $(\Delta P_{1-3})_j$. Figure 11 shows the calculated values of the axial momentum correction factor (k_{1-2}) and the branch loss coefficient (k_{1-3}), defined by [7] and [14] respectively, plotted against the branch flow split. The data shows clearly that a unique relationship exists between each of the two coefficients and the flow split ratio independent of mass flux. Using the least-squares method, the present data were correlated by

$$k_{1-2} = 0.704 - 0.320\left(\frac{\dot{m}_3}{\dot{m}_1}\right) - 0.028\left(\frac{\dot{m}_3}{\dot{m}_1}\right)^2 \qquad [21]$$

and

$$k_{1-3} = 1.081 - 0.914\left(\frac{\dot{m}_3}{\dot{m}_1}\right) + 1.050\left(\frac{\dot{m}_3}{\dot{m}_1}\right)^2. \qquad [22]$$

Although the limit for k_{1-2} should approach unity when ($\dot{m}_3/\dot{m}_1$) approaches zero, [21] represents the best fit of the data in the range $0.1 \leqslant \dot{m}_3/\dot{m}_1 \leqslant 1.0$. As shown in figure 11, the results of the present work for k_{1-3} agreed very well with those of Collier (1976) and Reimann & Seeger (1986). Collier (1976) and Reimann & Seeger (1986) presented empirical correlations for $\bar{k}_{1-2}$, as defined by [8], which is based on a mechanical energy balance model. When the present data were reduced by the same model good agreement was also obtained for flow splits >0.2.

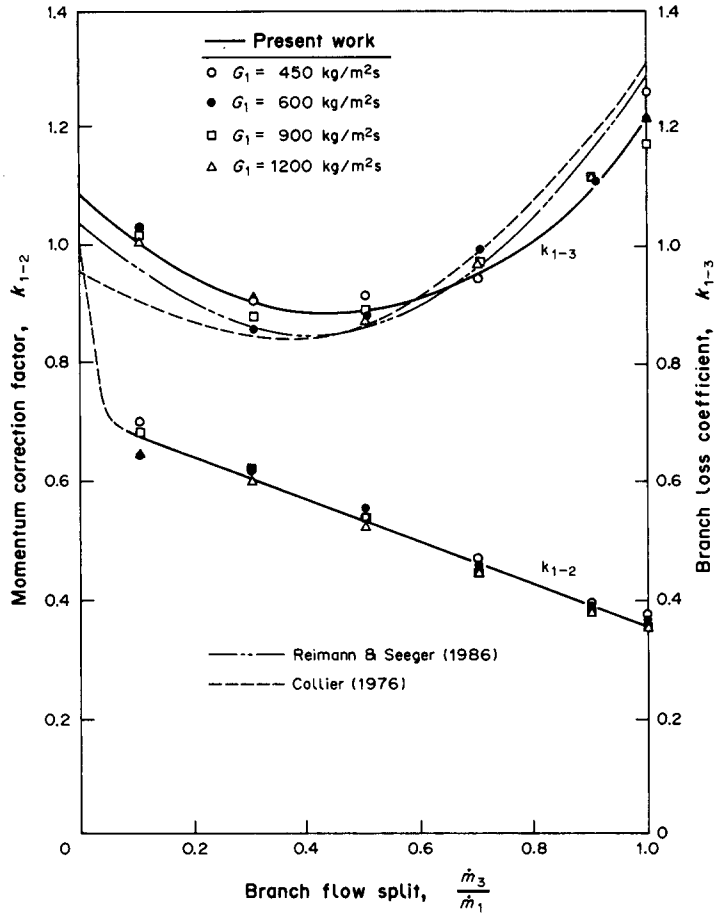

Figure 11. Single-phase momentum correction factor and branch loss coefficient vs flow split.

It must be noted that the balance of axial momentum [7] was used to model the pressure recovery in the run rather than the mechanical energy balance [8], which has been used by other investigators. The physical situation encountered as the flow passes the junction through the run is viewed as similar to the pressure rise due to a sudden expansion. Experimental evidence has shown that this is better predicted by a momentum balance based model, as was discussed by Delhay (1981).

The data presented herein were also consistent with the early data of McNown (1954), as was shown by Ballyk (1986).

5.2. Two-phase flow

A typical pressure distribution for stream–water dividing flows is shown in figures 10a and 10b. By examining similar plots for all the experimental runs, the strong interdependence of phase separation phenomenon and the pressure distributions was revealed. It was clear that as total phase separation was approached, a significant increase in the run pressure recovery was encountered. This sudden pressure change was always associated with flow regime transition from annular to plug flow in the run of the T-junction. The results of the present work for steam–water annular flow are analysed and compared with existing models in the following two sections.

5.2.1. Axial pressure recovery. The data on pressure recovery in the run were reduced to the homogeneous momentum correction factor ($k_{(1-2)H}$) using [11]. Figure 12 shows typical results for a sample of the data showing the effect of inlet quality on the relationship between $k_{(1-2)H}$ and the flow split ratio ($\dot{m}_3/\dot{m}_1$). Although no apparent correlation can be deduced from this figure, a notable increase in the value of $k_{(1-2)H}$ can be seen in the range of flow splits associated with total separation (i.e. $0.2 < \dot{m}_3/\dot{m}_1 < 0.3$). This phase separation condition was always associated with a

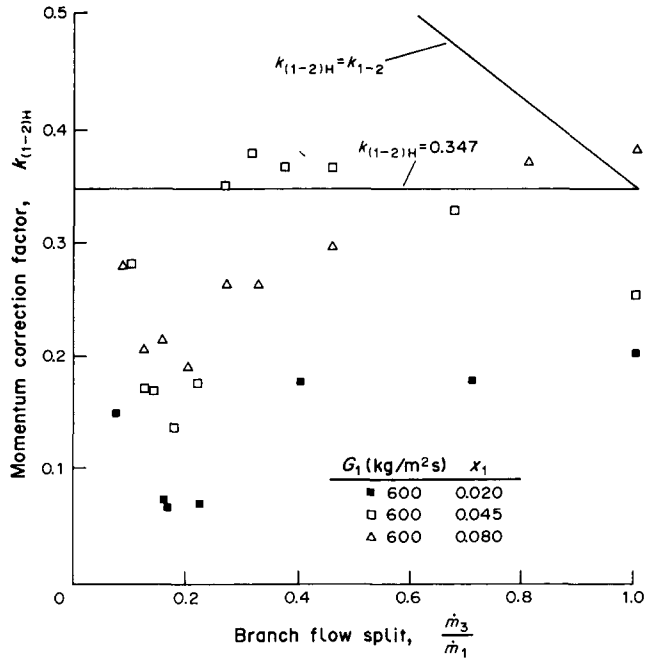

Figure 12. Homogeneous momentum correction factor vs flow split ($G_1 = 600\ \text{kg/m}^2\text{s}$).

flow regime transition to slug and plug flow in the run of the T-junction. The sudden increase in the calculated values of $k_{(1-2)H}$ can then be related to the inability of the homogeneous model to account for momentum changes resulting from a flow regime transition. All the axial pressure recovery data obtained in the present work demonstrated similar trends, as was shown by Shoukri *et al.* (1987).

Saba & Lahey (1984) suggested that the single-phase momentum correction factor (k_{1-2}) be used to predict two-phase pressure changes with the homogeneous model. For the data presented herein, the single-phase correction factor was always higher than the corresponding two-phase value except for high quality and high flow split ratios, as shown in figure 12. Fouda & Rhodes (1974) suggested that a constant value of 0.347 be used for $k_{(1-2)H}$.

The separated flow model [12] was also used to reduce the data using the measured values of void fraction in the inlet and run of the T-junction. The calculated values of the separated flow momentum correction factor ($k_{(1-2)s}$) for all the data obtained in the present work are given in figure 13. For flow splits near and beyond total separation, the momentum change across the junction associated with the flow regime transition was accounted for through the measured void fraction. As a result, the sudden change in the momentum correction factor in this range of flow split was not observed. The value of $k_{(1-2)s}$ appears to be distributed around 1.0, indicating that the axial momentum carried by the branching flow was insignificant. Similar results were obtained when the data was reduced using known void fraction correlations rather than the measured values. Obvious scatter around $k_{(1-2)s} = 1$ was present at low values of flow split ratios particularly for high inlet quality runs. At low flow splits, annular flow existed both upstream and downstream of the branch. Consequently, the flow momentum is relatively high in both the inlet and run. The comparatively small run pressure rise at low flow splits is then being correlated by a difference between two large valves. This, coupled with the measurement errors associated with high void fractions (low liquid volume fraction, $(1-\alpha)$, in [12]) is expected to cause the data scatter.

Fouda & Rhodes (1974) suggested a constant value of 0.533 be used for $k_{(1-2)s}$, which is generally lower than those obtained from the present work. This investigation was carried out with a branch-to-inlet diameter ratio < 1.0 and the void fractions used were determined from correlations rather then experimental measurements. These factors may account for the lack of agreement with the present results.

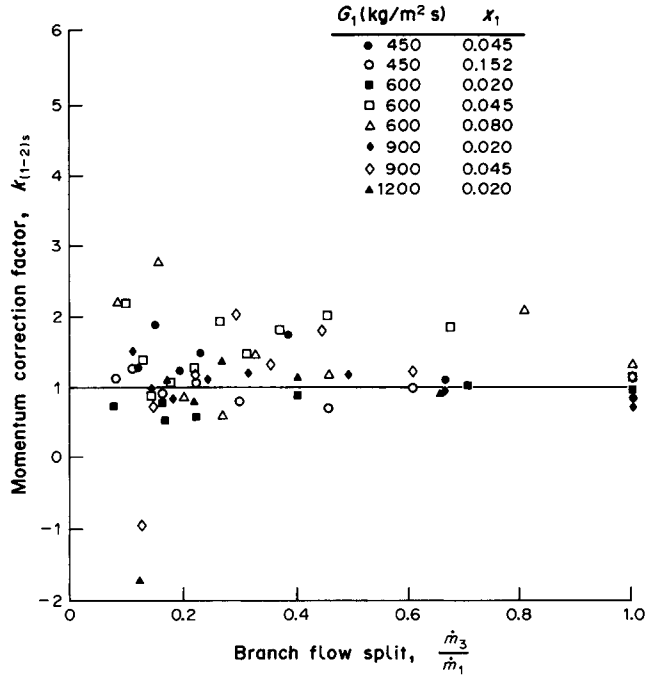

Figure 13. Separated flow momentum correction factor vs flow split.

Recently, Reimann & Seeger (1986) used a mechanical energy balance and a simplified momentum balance to obtain the following relationship for the run pressure recovery:

$$(\Delta P_{1-2})_j = \frac{\rho_{H2}}{2\rho_L^2}\left\{G_2^2\left[x_2\left(\frac{\rho_L}{\rho_G}\right)+(1-x_2)\right]^2 - G_1^2\left[x_1\left(\frac{\rho_L}{\rho_G}\right)+S_1(1-x_1)\right]^2\left[x_2+\frac{1-x_2}{S_1^2}\right]\right\}$$
$$+\frac{G_2^2}{\rho_L}\left\{\left[x_2\left(\frac{\rho_L}{\rho_G}\right)+S_2(1-x_2)\right]\left[x_2+\frac{1-x_2}{S_2}\right]-\frac{1}{C_2}\left[x_2\left(\frac{\rho_L}{\rho_G}\right)+(1-x_2)\right]\right\}, \quad [23]$$

where S is the slip ratio and C_2 is defined by

$$C_2 = \left[1+\left(\frac{\rho_{H1}}{\rho_{H2}}\right)^{0.5}\frac{V_1}{V_2}\sqrt{\bar{k}_{1-2}}\right]^{-1}. \quad [24]$$

Here, V_1 and V_2 are the inlet and run volumetric flow rates and $\bar{k}_{1-2}$ is the single-phase coefficient defined by [8]. Reimann & Seeger suggested known empirical correlations for estimating the slip ratios. The results of the present work were compared with the predictions of [23] using the suggested slip correlations. The comparisons are shown in figure 14. Agreement between the present data and Reimann & Seeger's correlation is seen to be poor, particularly for low split ratios. The same level of agreement was obtained when the measured slip ratios were used with [23].

5.2.2. Branch pressure drop. The data obtained in the present work were reduced using the mechanical energy model given by [15]. Similar to the axial pressure recovery, two methods were used for data reduction. Using the homogeneous model, for which the homogeneous density (ρ_H) replaced the energy weighted density (ρ''') in [15], the branch homogeneous pressure drop multiplier (Φ_H) was calculated. By using the separated flow model, for which the measured void fractions were used in conjunction with [15] and [16], the branch separated flow multiplier (Φ_s) was calculated. The results obtained did not agree with any of the available correlations ([17]–[20]), as was shown by Shoukri *et al.* (1987). One of the reasons for disagreement was the inability of the mechanical energy model, as formulated by [15], to account for the inlet dynamic head of the branching flow. An improvement on the mechanical energy based models can be achieved by correctly accounting for this term. The mechanical energy model is based on dividing the branch pressure change at the junction, $(\Delta P_{1-3})_j$, into reversible and irreversible components. This is obtained by first assuming the inlet mixture to be discontinuously divided into two streams just

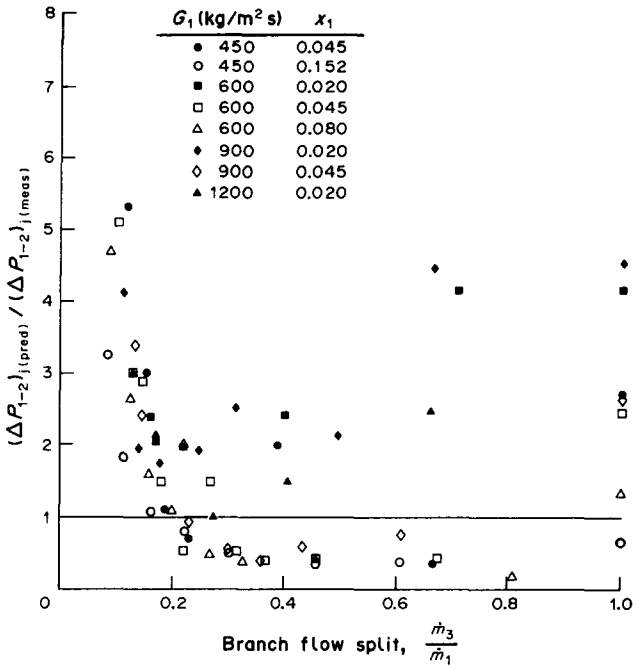

Figure 14. Ratio of predicted (Reimann & Seeger 1986) to measured run pressure change.

before the junction, as shown in figure 15. The reversible pressure change in the branch can then be modelled by way of a Bernoulli-type equation, as given by Lahey & Moody (1977), in the form

$$(P_{1j} - P_{3j})_{rev} \cdot \frac{\dot{m}_3}{\rho_{H3}} = \tfrac{1}{2}\dot{m}_{G3}(u_{G3}^2 - u_{G1}^2) + \tfrac{1}{2}\dot{m}_{L3}(u_{L3}^2 - u_{L1}^2), \qquad [25]$$

which is similar to [19] from Reimann & Seeger (1986). The phasic velocities are given by

$$u_G = \frac{Gx}{\alpha\rho_G} \quad \text{and} \quad u_L = \frac{G(1-x)}{(1-\alpha)\rho_L}. \qquad [26]$$

Equation [25] can therefore, be written as

$$(P_{1j} - P_{3j})_{rev} = \frac{\rho_{H3}}{2}\left\{G_3^2\left[\frac{x_3^3}{\alpha_3^2\rho_G^2} + \frac{(1-x_3)^3}{(1-\alpha_3)^2\rho_L^2}\right] - G_1^2\left[\frac{x_1^2 x_3}{\alpha_1^2\rho_G^2} + \frac{(1-x_1)^2(1-x_3)}{(1-\alpha_1)^2\rho_L^2}\right]\right\}. \qquad [27]$$

The first term between square brackets in [27] corresponds to the branch energy density (ρ_3''') defined earlier by [16], while the second term corresponds to the equivalent inlet density (ρ^*) which

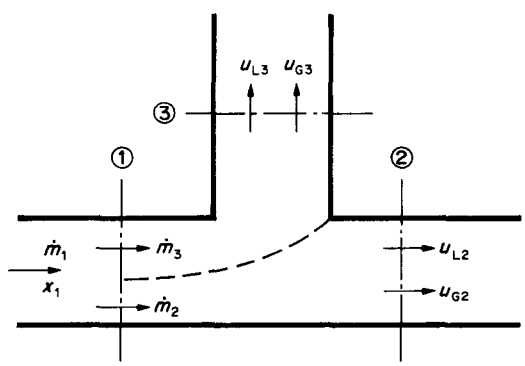

Figure 15. Junction model.

is consistent with the model assumptions. Equation [27] can be rewritten as

$$(P_{1j} - P_{3j})_{rev} = \frac{\rho_{H3}}{2}\left\{\frac{G_3^2}{(\rho_3''')^2} - \frac{G_1^2}{(\rho_1^*)^2}\right\}, \quad [28]$$

where ρ_3''' is defined by [16] and ρ_1^* is defined by

$$\frac{1}{(\rho_1^*)^2} = \frac{(1-x_1)^2(1-x_3)}{(1-\alpha_1)^2\rho_L^2} + \frac{x_1^2 x_3}{\alpha_1^2\rho_G^2}. \quad [29]$$

By assuming $\rho_1^* = \rho_1'''$, [28] reduces to the reversible portion of [15], as used by Saba & Lahey (1984).

Following the usual procedure of defining the irreversible junction pressure loss as a function of the inlet dynamic head, it is then appropriate to use the equivalent inlet density (ρ_1^*) to determine the loss multiplier. Therefore, the total branch pressure change at the junction becomes

$$(\Delta P_{1-3})_j = \frac{\rho_{H3}}{2}\left[\frac{G_3^2}{(\rho_3''')^2} - \frac{G_1^2}{(\rho_1^*)^2}\right] + k_{1-3}\frac{\rho_{H3}}{2}\frac{G_1^2}{(\rho_1^*)^2}\Phi^*, \quad [30]$$

from which a new multiplier, Φ^*, is defined. The limit of Φ^* is 1 as $G_3/G_1 \to 0$.

The usefulness of the model represented by [30] was demonstrated using the present data. All the data obtained were reduced based on [30] to calculate the two-phase multiplier Φ^* using the measured void fractions. The results showed that, for a given junction geometry, the multiplier Φ^* was a unique function of the split ratio ($\dot{m}_3/\dot{m}_1$), independent of both the inlet mass flux and inlet quality, as shown in figure 16. The strong dependence of other multipliers on the inlet quality was completely accounted for through the use of an equivalent inlet density term compatible with the usual mechanical energy based model for branch pressure drop. The data was used to obtain the following empirical correlation for Φ^*:

$$\Phi^* = -1.37 + 23.38\frac{\dot{m}_3}{\dot{m}_1} - 17.00\left(\frac{\dot{m}_3}{\dot{m}_1}\right)^2 + 1.12\left(\frac{\dot{m}_3}{\dot{m}_1}\right)^3, \quad \text{for} \quad \frac{\dot{m}_3}{\dot{m}_1} > 0.1. \quad [31]$$

It is expected that such a correlation will be dependent on the branch-to-inlet diameter ratio. The data showed similar trends when empirical void fraction correlations were used with [30].

Based on the present work, it is recommended that [30] be used to model the branch pressure changes. For low-pressure steam–water annular flow, [31] is recommended for evaluating the two-phase irreversible branch multiplier for a branch-to-inlet diameter ratio of unity.

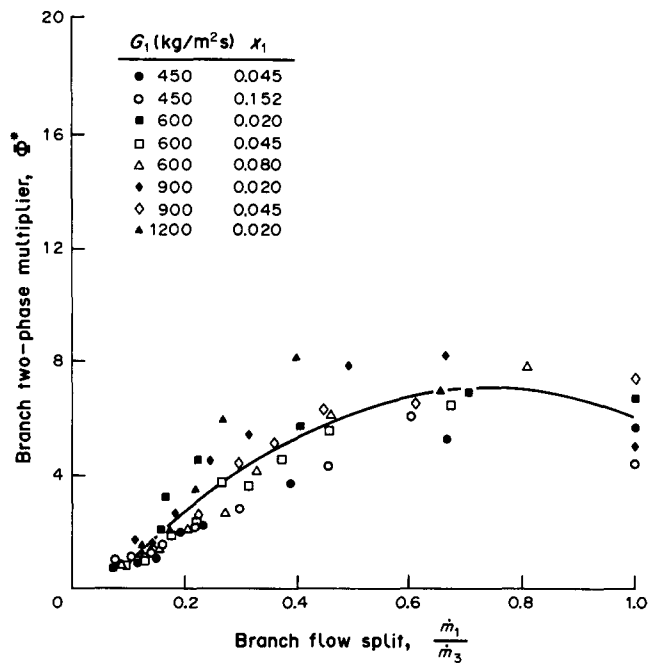

Figure 16. Branch two-phase multiplier vs flow split.

6. CONCLUSIONS

Extensive data for steam–water annular flow in a horizontal T-junction with a horizontal branch were obtained for different conditions of inlet mass flux, inlet quality and flow split ratio. The data covered a range of operating conditions which was not examined before. The data included detailed phase separation and pressure characteristics in the branching junction. A unique feature of the experiments was the measurement of the void fraction profiles along the three legs of the junction. The data obtained can, consequently, serve as benchmark data for model development.

For the flow conditions considered herein, separation effects were seen to be severe with the gas phase preferentially entering the branch. An assumption of complete phase separation in the junction closely approximated the data when more than 30% of the inlet flow was removed through the branch. Below 30% removal rate, the degree of phase separation was strongly dependent on the flow split ratio, inlet quality and, to a lesser extent, the inlet mass flux. The phase separation results obtained were consistent and complementary to the existing data base.

Based on the data obtained in the present work, the use of the separated flow axial momentum balance [12] is recommended for modelling the axial pressure recovery in piping junctions. Under the conditions tested herein, the average value of the pressure recovery coefficient, $k_{(1-2)s}$, was approximately unity, independent of flow conditions. This indicates that the axial momentum associated with the branching flow was insignificant.

A consistent model, based on a mechanical energy balance, was introduced to account for the pressure changes in the branch. The model resulted in the definition of a new two-phase branch loss multiplier accounting for the branch irreversible losses. Based on the present data, the two-phase multiplier was found to be dependent only on the flow split ratio for a given geometry and independent of inlet flow conditions. The data were used to empirically correlate the two-phase branch loss multiplier with the flow split ratio.

Acknowledgement—The work presented in this paper was funded by the Canadian Electrical Association (CEA No. 325-G430).

REFERENCES

AZZOPARDI, B. J. & FREEMAN-BELL, G. 1983 The effect of side arm diameter on the two phase flow split at a T-junction. Report AERE-M3290.

AZZOPARDI, B. J. & WHALLEY, P. B. 1982 The effect of flow patterns on two-phase flow in a T-junction. *Int. J. Multiphase Flow* **8,** 491–507.

BALLYK, J. D. 1986 On the characteristics of dividing steam–water flow in a horizontal tee junction. M.Engng Thesis, McMaster Univ., Hamilton, Ontario.

COLLIER, J. G. 1976 Single-phase and two-phase flow behaviour in primary circuit components. In *Proceedings of NATO Advanced Institute on Two-phase Flow and Heat Transfer*, Vol. 1, pp. 313–365. Hemisphere, Washington, D.C.

DELHAY, J. M. 1981 Singular pressure drops. In *Two-phase Flow and Heat Transfer in the Power and Process Industries*, Chap. 4 (Edited by BERGLES, A. E. *et al.*). Hemisphere, Washington, D.C.

FOUDA, A. E. 1975 Two-phase flow behaviour in manifolds and networks. Ph.D. Thesis, Dept of Chem. Engng, Univ. of Waterloo, Ontario.

FOUDA, A. E. & RHODES, E. 1974 Two-phase annular flow stream division in a simple tee. *Trans. Instn chem. Engrs* **52,** 354–360.

HENRY, J. A. R. 1981 Dividing annular flow in a horizontal tee. *Int. J. Multiphase Flow* **7,** 343–355.

HONG, K. C. 1978 Two-phase flow splitting at a pipe tee. *J. Petrol. Technol.* 290–296.

JOHANSEN, S. E. 1979 Experimental study of gas–liquid flow in a pipe tee. M.Sc. Thesis, Univ. of Tulsa, Okla.

LAHEY, R. J. JR & MOODY, F. J. 1977 The thermal-hydraulics of boiling water reactors. ANS Monograph.

MCNOWN, J. S. 1954 Mechanics of manifold flow *Trans. ASCE 2714* **119,** 1103–1142.

REIMANN, J. & SEEGER, W. 1986 Two-phase flow in a T-junction with a horizontal inlet—Part II: pressure differences. *Int. J. Multiphase Flow* **12,** 587–608.

RUBEL, M. 1986 Experimental investigation of phase distribution in a horizontal tee junction. M.Sc. Thesis. Univ. of Manitoba, Winnipeg.

SABA, N. & LAHEY, R. T. JR 1982 Phase separation phenomena in branching conduits. Report NUREG/CR-2590.

SABA, N. & LAHEY, R. T. JR 1984 The analysis of phase separation phenomena in branching conduits. *Int. J. Multiphase Flow* **10,** 1–20.

SEEGER, W., REIMANN, J. & MÜLLER, U. 1986 Two-phase flow in a T-junction with a horizontal inlet—Part I: phase separation. *Int. J. Multiphase Flow* **12,** 575–585.

SHOUKRI, M., BALLYK, J. D. & CHAN, A. M. C. 1987 On the characteristics of two-phase flow in network branches. Canadian Electrical Association (CEA) Report 325G430.